Dual pH Responsive Macrophage Targeted Isoniazid Glycoparticles as Intracellular Tuberculosis Therapy

Andrew M. Lunn [a], Meera Unnikrishnan [b] & Sébastien Perrier* [a,c]

a Department of Chemistry, The University of Warwick, Gibbet Hill, Coventry, CV4 7AL, UK
b Division of Biomedical Sciences, Warwick Medical School, University of Warwick, Coventry, UK
c Faculty of Pharmacy and Pharmaceutical Sciences, Monash University, 381 Royal Parade, Parkville, VIC 3052, Australia

*s.perrier@warwick.ac.uk

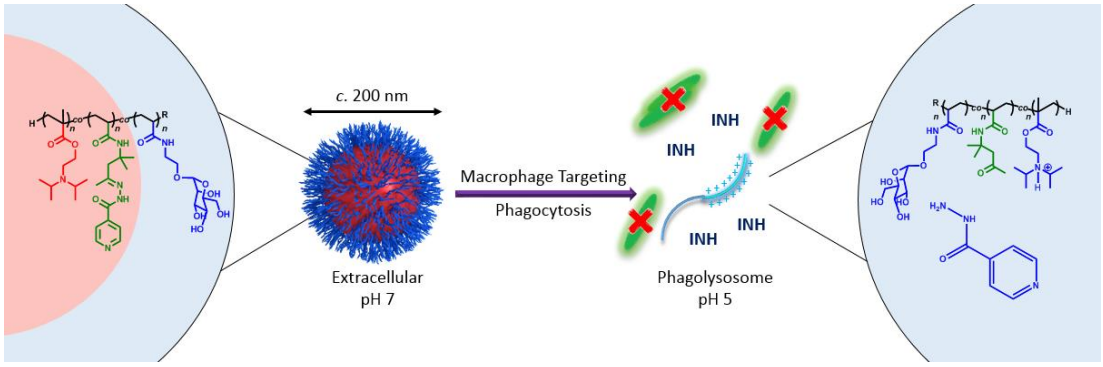

Abstract

Tuberculosis (TB) is a global epidemic that kills over a million people every year, particularly in low resource communities. *Mycobacterium tuberculosis*, the most common bacterium that causes TB, is difficult to treat particularly in its latent phase, in part due to its ability to survive and replicate within the host macrophage. New therapeutic approaches resulting in better tolerated and shorter antibiotic courses that target intracellular bacteria are critical to effective treatment. The development of a novel, pH responsive, mannosylated nanoparticle, covalently linked with isoniazid, a first line TB antibiotic, is presented. This nanoparticle drug delivery agent has increased macrophage uptake and, upon exposure to the acidic phagolysosome, releases isoniazid through hydrolysis of a hydrazone bond, and disintegrates into a linear polymer. Full antibiotic activity is shown to be retained, with mannosylated isoniazid particles being the only treatment exhibiting complete bacterial eradication of intracellular bacteria, compared to an equivalent PEGylated system and free isoniazid. Such a system, able to effectively kill intracellular mycobacteria holds promise for improved outcomes in TB infection.

Introduction

Tuberculosis (TB), a serious bacterial infection mainly caused by *Mycobacterium tuberculosis*, is one of the top 10 causes of death in the world, killing 1.7 million people in 2016 alone.[1] Most infections affect the lungs, and disease transmission generally occurs *via* prolonged inhalation of aerosols from an actively infected person. Infection typically occurs whilst living in close quarters, with most cases occurring in countries with low or middle incomes[2,3]. One of the most widely used antibiotics in the treatment of TB is isoniazid, commonly in combination with rifampicin, pyrazinamide or ethambutol, for a minimum of six months in active infection; and as monotherapy in latent infection[4-6]. One of the reasons for such long drug regimens is poor penetration of the drug into sites of infection within tissues. *M. tuberculosis* replicates and

survives within immune cells such as macrophages within lung granulomas [7-11]. Ineffectiveness of current TB treatments is also due to patients not completing long antibiotic courses, which can be up to 12 months in duration[12, 13]. New therapeutics, capable of effectively targeting intracellular bacteria would therefore be an invaluable weapon in combatting tuberculosis, in particular for latent infections.

Many strategies exist to improve tuberculosis therapy, including the development of novel antibiotics such as bedaquiline[14-17]. Another approach, with potential to quickly improve the efficacy and longevity of current antibiotics, is to deliver antibiotics to the site of action in a targeted nanocarrier[18-20]. In this manner an increased concentration of antibiotic may be achieved at the infection site, in this case the macrophage, from a smaller overall administered dose, potentially reducing systemic exposure and minimising associated side effects. Many nanoparticle systems for drug delivery that are currently under study are polymeric in nature; these systems may be synthesised with a range of functional monomers using techniques such as emulsion polymerisation[21-24], which provides an industrially applicable way of generating polymeric nanoparticles with narrow size distributions[25, 26].

A classic emulsion polymerisation utilises a charged surfactant, such as sodium dodecyl sulfate, to form micelles, providing nucleation sites of insertion for growing "z-mer" polymer chains and stabilisation to the growing particles[27]. This allows for the synthesis of polymer nanoparticles at a high weight percentage, with diameters routinely below 100 nm. The presence of such a surfactant though, is detrimental for many medicinal uses, and requires extensive dialysis to be removed[28-30]. Avoiding the need for surfactant removal is one motivating factor behind the development of "pseudo-surfactant free" controlled radical polymerisation techniques such as RAFT emulsion polymerisation [31-36]. Such techniques whilst promising, suffer from having a relatively high associated material cost, and biocompatibility issues[37, 38]. Research conducted in the 1970's before the advent of controlled radical polymerisation techniques, investigated the use of a classical emulsion polymerisation without the addition of a surfactant to the system creating a self-nucleating "free radical surfactant free" emulsion polymerisation[39-42]. In such a system one or many of growing "z-mer" chains, nucleate into a growing polymer particle by collapsing out of solution on themselves, stabilised by the water-soluble initiator head groups. This produces both polymer in solution, and suspended polymer particles, with charged initiators facilitating access to sub-100 nm diameters[43-50]. More recently it has been shown that the addition of a suitable hydrophilic monomer into the emulsion polymerisation, produces functionalised nanoparticles in a simple three hour synthesis from monomer to final latex[51]. Such a technique, without the addition of surfactant or costly initial polymer synthesis, represents an attractive means by which to produce a nanocarrier.

Any nanocarrier must be able to be effectively loaded with a drug and release it at the intended site of action, in this case intracellularly in the macrophage. Covalently loading a drug to a nanocarrier is one way of ensuring high drug loading with minimal unwanted release. If this strategy is employed, the covalent bond must be cleavable at the site of action, and a release trigger of considerable interest is pH, particularly when targeting the macrophage, as upon phagocytosis a shift in environment from extracellular pH 7 to lysosomal pH 5 would be experienced[52, 53]. Such a change would quickly hydrolyse a bond such as an imine, oxime or hydrazone, and consequently release any drug tethered by it e.g. isoniazid[54-56].

The same pH shift could also be used to address one further issue when using polymeric nanoparticles for drug delivery, the accumulation of the injected particles in organs such as the liver and spleen[57]. If such a pH shift could induce particles to break up into their constituent polymers, this would result in material that is able to be cleared[58-62]. Poly(2-

(Dimethylamino)ethyl methacrylate) (P(DMAEMA)) has been shown able to switch solubility from hydrophobic to hydrophilic upon pH reduction, due to protonation of the pendant tertiary amine[63-65]. It is reasonable to assume that similar polymers bearing a tertiary amine such as poly(2-(di-isopropylamino)ethyl methacrylate) (P(DPAEMA)) would exhibit similar behaviour. If this solubility change could be induced at lysosomal pH, such polymers could be used to produce the required particle break-up to avoid accumulation.

Various properties are known to affect macrophage uptake of particles, including (though not limited to) surface charge, mechanical deformation and size. The role of these properties is complex, however macrophages have been shown to preferentially phagocytose particles ≥100 nm in diameter, making this a reasonable cut of point in the physical design of macrophage targeting nanocarriers[66-69]. Macrophages also express cell surface lectins such as Dendritic Cell-Specific Intercellular adhesion molecule-3-Grabbing Non-integrin (DC-SIGN) and CD206, which bind to the sugar α-D-mannose, a property that can be taken advantage of by coating the surface of a nanocarrier with mannose containing polymers[70-73]. Lectin-sugar interactions have previously been shown to be enhanced by the close packing of sugars such as on a particle surface, the "cluster glycoside effect"[74-77]. Thus mannose coated polymeric nanoparticles are good candidates for targeting the macrophage, a key niche for *M. tuberculosis* during infection.

Here, we present the synthesis of isoniazid linked nanoparticles synthesised *via* a free radical-surfactant free emulsion polymerisation technique with a novel hydrazone linked, pH responsive isoniazid vinyl monomer (DAAm-*hydrazone*-INH) together with: Di-isoPropyl Amino Ethyl MethAcrylate (DPAEMA) and Mannopyran-1-oxyethyl Acrylamide (ManAm).[51] We further demonstrate that particles with a mannose shell are capable of preferential endocytosis into macrophage cells, and upon endocytosis, release their antibiotic cargo as a result of acidic hydrolysis of the hydrazone linker. Furthermore, this reduction in pH causes the particles to break down into their constituent linear polymers. Finally, bacterial killing assays show the retention of antibiotic activity after intracellular release, with complete eradication of intracellular mycobacteria achieved only by mannose coated, pH-responsive isoniazid nano-carrier.

Results

Synthesis of pH responsive, non-responsive and fluorescent monomers.

To achieve intracellular release of isoniazid with a high drug loading and efficiency, a responsive monomer was required that was suitable for use during emulsion polymerisation, and able to release isoniazid upon phagocytosis. The pH change from the extracellular to phagoloysosomal environment is from around pH 7 to 5. As isoniazid bears a hydrazine group, a convenient bond that this can form with an aldehyde or ketone is a hydrazone, which is stable at pH 7 and hydrolyses around pH 5. To achieve this hydrazone linked monomer, a condensation reaction was performed between the hydrazine group on isoniazid, and the ketone on the commercially available monomer, diacetone acrylamide. Using stoichiometric conditions, the reaction yielded in full conversion the expected structure of the diacetone acrylamide-isoniazid imine linked monomer (DAAm-*hydrazone*-INH) product. The structure was confirmed by ^{1}H NMR spectroscopy, mass spectrometry and elemental analysis. (Figure S1)

To assess the pH-responsive isoniazid release of the DAAm-*hydrazone*-INH monomer, a non-responsive control was also synthesised that would not release isoniazid at the reduced phagolysosomal pH. This was achieved by coupling the hydrazine group on isoniazid with 2-isocyanatoethyl methacrylate, forming a urea linked isoniazid monomer (*urea*-INH). The pure

monomer was found to precipitate out of methanol when cooled to 2-8 °C, and was recovered by filtration and further purified by recrystallization in methanol. The structure and purity were confirmed by ^{1}H NMR spectroscopy, mass spectrometry and elemental analysis (Figure S2). By having both a pH and non-pH responsive monomer, particles could then be made that were suitable for assessing the ability of a hydrazone linked isoniazid for intracellular release.

In order to determine particle uptake by macrophages however, a fluorescent particle analogue was required to track the particles by fluorescence microscopy and using a fluorescence plate reader. To produce fluorescent particle analogues, a cyanine 3 acrylamide (Cy3Am) monomer was synthesised to be used as a co-monomer in a low molar percentage during particle synthesis. To achieve this, Cyanine 3 amine was reacted with acryloyl chloride; mass spectrometry and HPLC analysis revealed that this resulted in a pure Cy3Am monomer suitable for use as a hydrophilic co-monomer during emulsion polymerisation. (Figure S3). Having synthesised all required monomers, both pH responsive and non-pH responsive isoniazid linked particles could be synthesised with their fluorescent analogues.

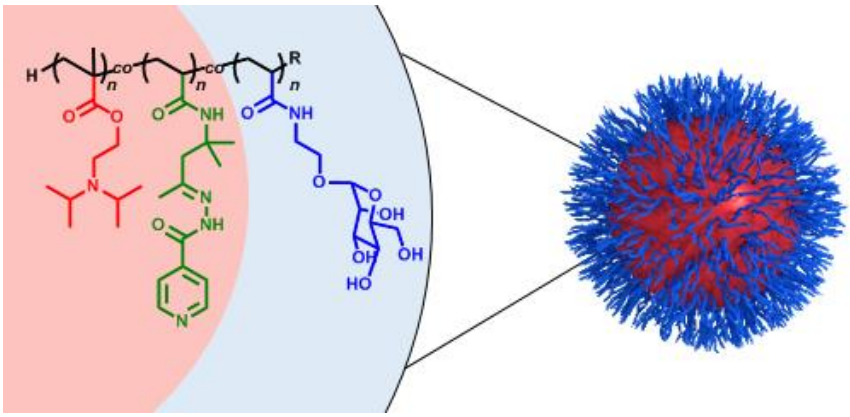

Figure 1: Graphical representation of the nanoparticle system produced showing the three components: poly(mannopyran-1-oxyethyl acrylamide) in blue, poly(diisopropylamino)ethyl methacrylate)) in red and poly(diacetone acrylamide-*hydrazone*-isoniazid) in green

Particle synthesis

To produce controlled drug delivery to macrophages, nanoparticles around 200 nm in diameter and coated in mannose were targeted. This was in order to exploit both the propensity of macrophages to phagocytose particles over 100 nm in diameter, and to target the cell surface lectins known to preferentially bind to mannose, such as DC-SIGN and CD206 [70-72, 78, 79]. The particles were synthesised using a free radical surfactant free emulsion polymerisation method previously published by the group[51]. In addition to the investigative system of mannose coated particles with cleavable isoniazid (P(ManAm)-*co*-P(DAAm-*hydrazone*-INH)-*co*-P(DPAEMA)) (Figure 1), control particles of: Mannose with no antibiotic (P(ManAm)-*co*-P(DPAEMA)), Mannose and a non-cleavable isoniazid (P(ManAm)-*co*-P(*urea*-INH)-*co*-P(DPAEMA)), PEGA shell with no antibiotic (P(PEGA)-*co*-P(DPAEMA)), and PEGA with cleavable isoniazid (P(PEGA)-*co*-P(DAAm-*hydrazone*-INH)-*co*-P(DPAEMA)) were also synthesised. This was to determine the source of any antimicrobial activity.

Particle	Hydrophilic Monomer (mol)	DPAEMA (mol)	Isoniazid monomer (mol)	Cy3 Am (mol)	Diameter (nm)	Pdi[c]	w/w% pro-drug loading[d]
P(ManAm)-*co*-P(DPAEMA)	$4.69x10^{-5}$	$6.33x10^{-5}$	n/a	n/a	210[a]	0.08	n/a
P(ManAm)-*co*-P(*urea*-INH)-*co*-P(DPAEMA)	$4.69x10^{-5}$	$8.44x10^{-5}$	$4.69x10^{-5}$	n/a	280[a]	0.04	48
P(ManAm)-*co*-P(DAAm-*hydrazone*-INH)-*co*-P(DPAEMA)	$4.69x10^{-5}$	$8.44x10^{-5}$	$4.69x10^{-5}$	n/a	212[a]	0.1	44
P(PEGA)-*co*-P(DPAEMA)	$4.69x10^{-5}$	$8.44x10^{-5}$	n/a	n/a	212[a]	0.14	n/a
P(PEGA)-*co*-P(DAAm-*hydrazone*-INH)-*co*-P(DPAEMA)	$4.69x10^{-5}$	$8.44x10^{-5}$	$4.69x10^{-5}$	n/a	225[a]	0.07	33
P(ManAm)-*co*-(DAAm-*hydrazone*-INH)-*co*-P(DPAEMA)-*co*-P(Cy3Am)	$4.69x10^{-5}$	$8.44x10^{-5}$	$4.69x10^{-5}$	$8.44x10^{-7}$	175[b]	0.1	43
P(PEGA)-*co*-P(DAAm-*hydrazone*-INH)-*co*-P(DPAEMA)-*co*-P(Cy3Am)	$4.69x10^{-5}$	$8.44x10^{-5}$	$4.69x10^{-5}$	$8.44x10^{-7}$	205[b]	0.04	33
P(ManAm)-*co*-P(DPAEMA)-*co*-(P(Cy3Am)	$4.69x10^{-5}$	$6.33x10^{-5}$	n/a	$6.33x10^{-7}$	131[b]	0.03	n/a

Table 1: Characterisation of all particles synthesised *via* surfactant free emulsion polymerisation, all reactions used a VA-044 initiator at a concentration of 0.75 mg mL^{-1}. [a] determined using DLS number distribution, [b] determined using SEM with an average of 20 particles measured, [c] determined using Equation 1. Original DLS traces see Figure S4, SEM images Figures S5-7, [d] determined using Equation 1.

Fluorescent analogues of P(ManAm)-*co*-(DAAm-*hydrazone*-INH)-*co*-P(DPAEMA)-*co*-P(Cy3Am), P(PEGA)-*co*-P(DAAm-*hydrazone*-INH)-*co*-P(DPAEMA)-*co*-P(Cy3Am) and P(ManAm)-*co*-P(DPAEMA)-*co*-P(Cy3Am) particles were also synthesised with 1% Cy3Am co-monomer as a molar ratio to DPAEMA content. All non-fluorescent latexes were analysed for particle size by DLS. Fluorescent latexes were analysed using SEM as DLS was not suitable due to absorption at the wavelength of the laser used (633 nm) (Table 1). Particle diameters are reported as number distributions, this has been previously found by the group to best match microscopy analysis and makes the sizes comparable to those reported for fluorescent particles[77]. The absorption/emission maxima of the Cy3Am particles was determined as 554/565 nm (Figure 2). There was some size discrepancy between particles, with the majority showing diameters of around 200 nm. Crucially the (P(ManAm)-*co*-P(DAAm-*hydrazone*-INH)-*co*-P(DPAEMA)), (P(ManAm)-*co*-P(DPAEMA)), (P(PEGA)-*co*-P(DAAm-*hydrazone*-INH)-*co*-P(DPAEMA)) and (P(PEGA)-*co*-P(DPAEMA)) particles were all within a 15 nm diameter range (210-225 nm). This is important as these particles were directly compared for their antibiotic activity in cell tests.

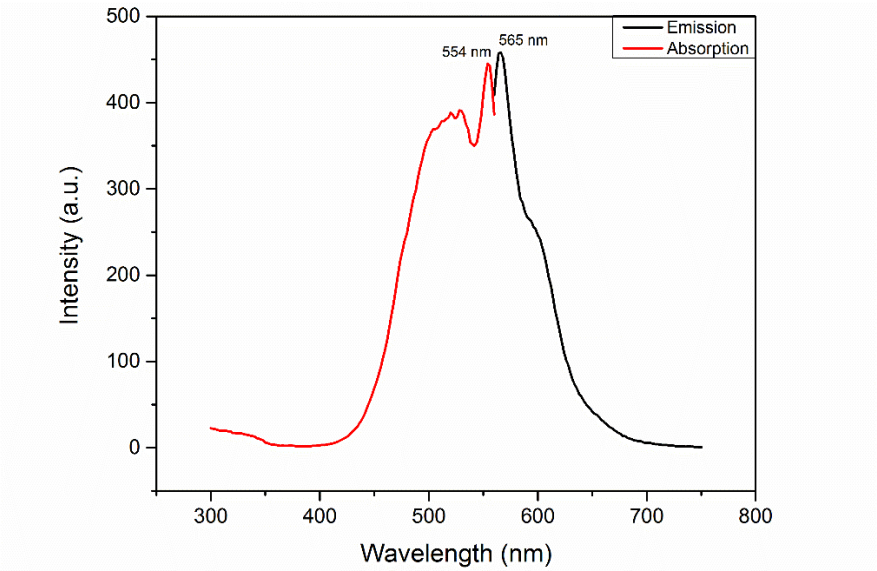

Figure 2: Fluorescent absorption and emission spectrum of Mannose-(DAAm-*hydrazone*-Iso)-DPAEMA-Cy3Am particles in water, absorption/emission maxima λ = 554/565 nm

Using this emulsion polymerisation method for isoniazid loading ensured 100% encapsulation efficiency as isoniazid was already covalently linked to the monomer, which is significantly higher than possible using entrapment methods, typically showing 40-80%.[80-82] Furthermore the pro-drug loading of DAAm-*hydrazone*-INH achieved in the investigative system of (P(ManAm)-*co*-P(DAAm-*hydrazone*-INH)-*co*-P(DPAEMA)) was 33 %, (pro-drug loading was used for continuity of calculation between systems and to account for change in mass of conjugate product). Both of these represent a high percentage of drug loading, compared to the commonplace loading percent achieved in the literature of around 10%[83]. This produced a latex with a final active isoniazid concentration of 6.5 mg mL^{-1}, which is potentially too low for clinical applications, however if the solids content of this emulsion were increased to the maximum of 15% as previously published, a concentration of 44 mg mL^{-1} could be achieved whilst still keeping a stable latex[51]. This concentration would be clinically relevant for both injectable and inhalable formulations with 6.8 mL providing a current standard dose of 300 mg isoniazid, suitable for IV injection or nebulisation[84]. This dose represents a "worst case scenario" in terms of drug delivery, as it is the intention of the presented drug delivery system to reduce the required total dose and treatment time.

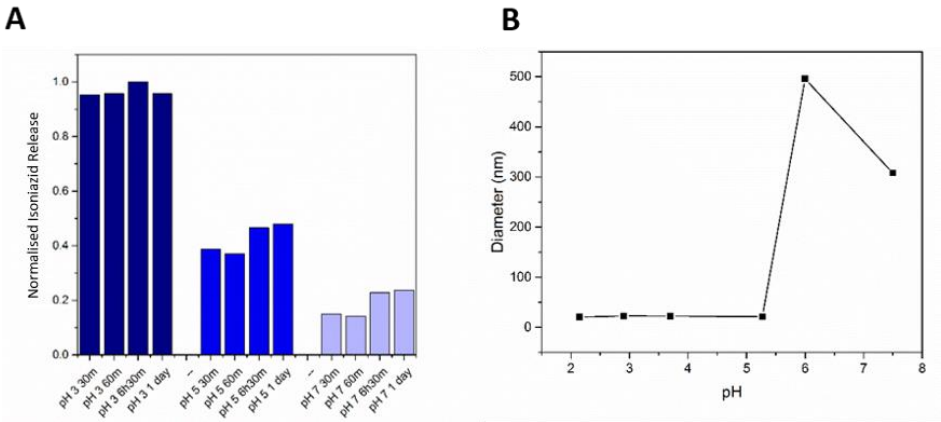

Figure 3: A) Normalised level of isoniazid released from P(ManAm)-*co*-P(DAAm-*hydrazone*-INH)-*co*-P(DPAEMA) particles over 24 hours at pH 3, 5 and 7, determined using HPLC (Original traces S9), B) Average diameter by DLS of P(ManAm)-*co*-P(DAAm-*hydrazone*-INH)-*co*-P(DPAEMA) particles at pH: 2.1, 2.9, 3.7, 5.3, 6 and 7.5, showing stability at pH 7 and particle break up as a large drop in diameter below pH 6, count rate data Figure S8

Particle disintegration and isoniazid release pH studies

For the synthesised particles to selectively release isoniazid intracellularly, it is necessary for the hydrazone bonding the isoniazid to be selectively cleaved, in response to a relevant drop in pH. To assess this and the ability of the particles to disassemble at reduced pH values, their physical characteristics at a range of pHs were first assessed. To determine if isoniazid would be released from the particles at a relevant pH, P(ManAm)-*co*-P(DAAm-*hydrazone*-INH)-*co*-P(DPAEMA) particles were diluted in phosphate buffered saline (PBS) to 1 mg mL^{-1} at pH: 3, 5 and 7 and analysed by HPLC over 24 hours, comparing peak integrations for isoniazid. HPLC samples were prepared by centrifugation to remove polymer particles (where still present) and filtration to remove as much polymer as possible. This purification was necessary as the acidic conditions of the HPLC eluent would cause hydrolytic release of isoniazid bound to any polymer left, producing an artificially increased release profile (Figure 3, S9). The results confirmed the release of isoniazid at reduced pH values, with the largest release of isoniazid being seen at pH 3, reducing to half at pH 5. Some limited release can be seen at pH 7; this is believed to be caused by residual particles/polymer in solution, releasing isoniazid in the acidic conditions of the HPLC eluent. These results confirmed that the DAAm-*hydrazone*-INH monomer was stable at neutral pH, releasing isoniazid *via* hydrolysis at reduced pH values. Whilst a higher percentage of release would be desirable, these results were in line with recent literature: Hwang *et al.* showed isoniazid release from a silica particle using a similar hydrazone linker to be stimulated with reduced pH, and minimal release at pH 7. More recently Nkanga *et al.* showed in two publications, nearly full isoniazid release from a hydrazone linker in 12 hours below pH 5.4[85-87].

A 5 mg mL^{-1} solution of the non-responsive *urea*-INH monomer was also tested for isoniazid release at pH 3 by mass spectrometry to ensure it was hydrolytically stable and a suitable control (Figure S10). After 24 hours, a characteristic peak for the *urea*-INH monomer at m/z 315.2 $[mass + Na]^+$ was still observed, with no trace of a peak for isoniazid. This result confirmed that the non-responsive control monomer did not release isoniazid under acidic physiological conditions.

Due to the tertiary amine becoming protonated in acidic conditions, DPAEMA is known to exhibit pH responsive behaviour, switching from hydrophobic to hydrophilic in an acidic environment[62, 88, 89]. For this reason it was chosen as a co-monomer for particle synthesis, in order to cause particle disintegration after endocytosis and avoid particle bioaccumulation. Dilutions of P(ManAm)-*co*-P(DAAm-*hydrazone*-INH)-*co*-P(DPAEMA) particles were prepared to pHs of: 2.1, 2.9, 3.7, 5.3, 6 and 7.5, and their diameter analysed by DLS to determine the pH at which particle break up occurred (Figure 3). The particles were shown to be stable from pH 7.5-6, below which the particles swelled and disintegrated; this can be seen as an increase and subsequent drop in diameter by DLS. The point of disassembly at pH 6, which represents the pK_b of the P(DPAEMA) is a useful value biologically, as the synthesised particles will be stable at extracellular pH 7 and break up in phagolysosomal conditions (around pH 5). The pH at which these particles break up is as expected and matches that reported by Xu *et al.* who used the same response to trigger the assembly of a polymeric tri-block[88]. These results confirmed the ability of this particle system to both break down into linear polymer and release isoniazid in response to a biologically relevant pH drop, and thus the suitability of the system for further biological testing as an intracellular drug delivery vector for isoniazid.

Cytotoxicity

In order for this particle system to be of use in delivering isoniazid to kill infective bacteria, it must itself be biocompatible and non-toxic to the host cells. To ensure the particles were

biocompatible, cell viability tests were performed to determine the cytotoxicity of the responsive particles synthesised. The equivalent concentration of isoniazid linked to the particles was used as a control. A 2,3-bis-(2-methoxy-4-nitro-5-sulfophenyl)-2H-tetrazolium-5-carboxanilide (XTT) assay was performed to determine cell viability by mitochondrial activity against a healthy cell control (Figure 4). Particles were tested against a lung epithelial cell line (A549) and PMA activated THP-1 macrophages, representative of the typical pulmonary environment. The particles were shown to be non-toxic up to 0.5 mg mL^{-1} of polymer against A549 cells and 0.1 mg mL^{-1} in macrophages. The equivalent dose of isoniazid showed a similar, but less pronounced trend in both cell lines; it may then be concluded that any cytotoxic effect seen from the isoniazid particles is predominantly due to the presence of polymer and partially isoniazid. This matches well with the literature, one useful example from Hwang *et al.* in 2016 tested a range of polymeric nanoparticles against A549 and THP-1 cells specifically and also reported significant toxicity above 0.1 mg mL^{-1} [90]. Taken together with physical tests, these results suggested that the particles were suitable for further biological testing.

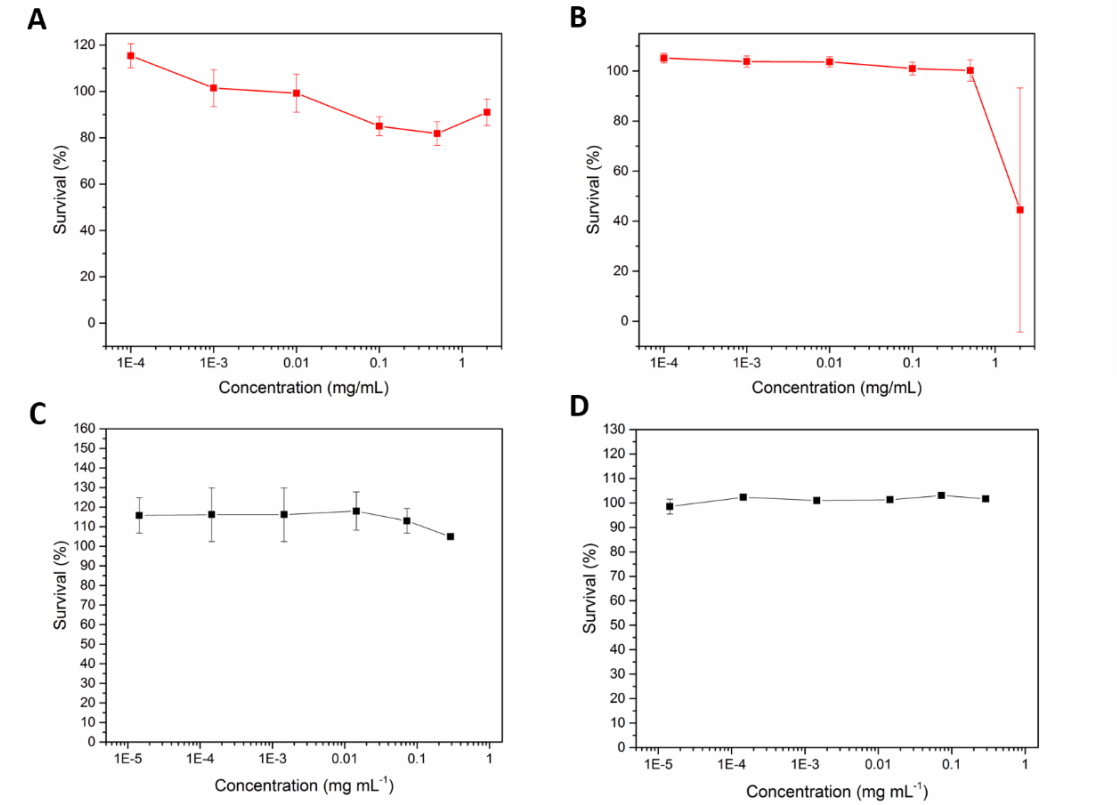

Figure 4: Cytotoxicity tests, cell viability determined over 24 hours using an XTT assay. P(ManAm)-*co*-P(DAAm-*hydrazone*-INH)-*co*-P(DPAEMA) particles tested against: A) THP-1 derived macrophages and B) lung epithelial (A549) cells. The equivalent concentrations of isoniazid delivered by the particle system tested against: C) THP-1 derived macrophages and D) lung epithelial (A549) cells

Preferential endocytosis of mannosylated particles into macrophages

It is important for the mechanism of particle break up and drug release that the particles are endocytosed *via* a lysosomal pathway, exposing the particles to an acidic environment. This has been previously demonstrated by Kalluru *et al.* who showed polylactide nanoparticles were trafficked to the phagolysosome of macrophages[91]. To test if the presence of mannose on the particle surface would confer a preferential endocytosis fluorescent cell uptake assays were performed using a Cytation 3 plate reader, with equivalent experiments performed using confocal fluorescence microscopy. Previously synthesised fluorescent particle analogues were

purified so that they had no free dye present that would interfere with the experiment. To achieve this, P(ManAm)- *co*-(DAAm-*hydrazone*-INH)-*co*-P(DPAEMA)-*co*-P(Cy3Am) and P(PEGA)-*co*-P(DAAm-*hydrazone*-INH)-*co*-P(DPAEMA)-*co*-P(Cy3Am) particles were purified by repeated cycles of centrifugation and replacement of supernatant with clean, deionised water. Both visually and using fluorescence spectroscopy, supernatants showed an eventual loss of fluorescence, and HPLC analysis of the purified particles showed loss of free fluorescent polymer and monomer after purification, confirming the successful removal of all free dye. (Figure S11).

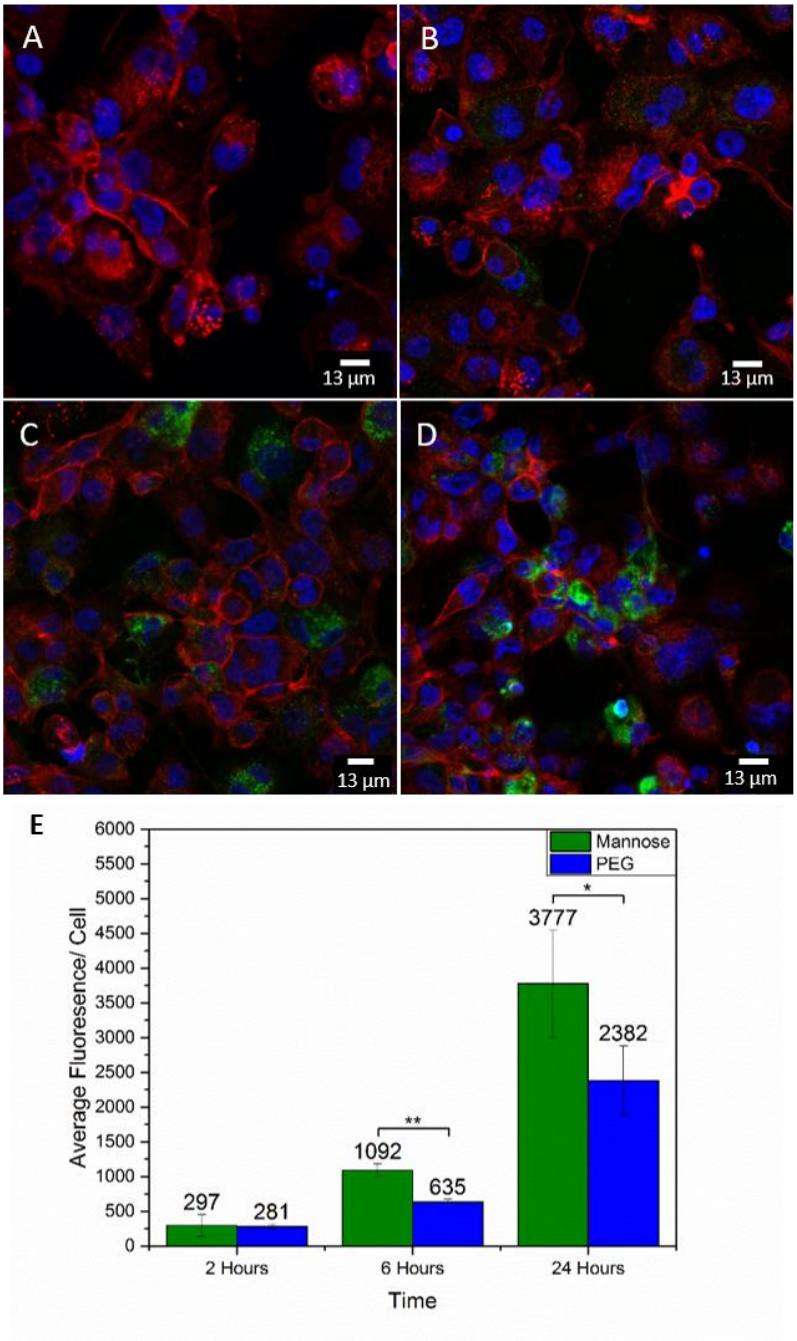

Figure 6: Cellular uptake of fluorescent analogues of P(ManAm)-*co*-(DAAm-*hydrazone*-INH)-*co*-P(DPAEMA)-*co*-P(Cy3Am) particles at 0.1 mg mL^{-1} by THP-1 derived macrophages tracked in A-D by confocal microscopy with particle incubation for B) two hours, C) six hours, D) 24 hours and A) as a control with no particles. Particles are shown in green with a Cy3 fluorophore, actin in red stained with DyLight 650 phalloidin, and the cell nucleus in blue stained with DAPI. E) Comparative uptake of fluorescent ManAm and PEGA particles. Average intracellular fluorescence was determined as an

indicator of endocytosis. Error bars show standard error, * = $p < 0.05$, ** = $p < 0.01$ determined by a Student's t-test. Representative images taken by Cytation plate reader shown in Figure S13.

The purified particles were then used in a fluorescence uptake assay. Particles were incubated at 0.1 mg mL^{-1} with THP-1 macrophage cells for two, six and 24 hours. The level of intracellular fluorescence was measured, taking an average reading of fluorescence per cell as an indication of the level of endocytosis (Figure 6) (Representative images taken by the plate reader are shown in Figure S13). The relative fluorescence of the two latexes were normalised to each other using the extinction coefficient of each, obtained from calibration curves of fluorescence by concentration (Figure S12).

The results showed that the particles were taken up in a time dependent manner and that, at six and 24 hours, a significantly increased fluorescence was observed for the mannose coated particles. This confirmed that a mannose shell conferred a preferential endocytosis over PEGA equivalent. These statistical analyses were supplemented with confocal microscopy analysis of the mannose coated particles uptake by THP-1 macrophages, and showed punctuated fluorescence increasing in intensity over the same time course (Figure 6). Providing evidence that the presence of a mannosylated shell does confer a preferential uptake into macrophage cell lines.

The increased endocytosis on mannosylated particles, though statistically significant is modest, as those with a PEG shell also show a time dependant increase in uptake. This effect has been reviewed in the literature, and the results presented here are broadly in line with previously reported data, with mannosylated liposomes having been shown to have an increased macrophage uptake when compared to a "bare" liposomal equivalent[92]. The relative increase in mannosylated particle uptake, compared to a PEG equivalent in the environment of a well plate with a cell monolayer, is not surprising. In this artificial environment the macrophages are left with particles simply placed on them in a perfect environment for their growth. The situation *in vivo* though is rather more complex, as the targeting of mannose receptors may give a far more pronounced increase in macrophage uptake. Reports regarding the *in vivo* uptake of a mannosylated compared to non-mannosylated particles all show an increased macrophage uptake of mannosylated particles, although the extent to which that effect is seen varies greatly between reports.[72, 93, 94] Indeed some studies, such as that from the Hashida group report a *circa* two fold increase in alveolar macrophages,[67] with others including those from the Morimoto group showing almost a three-fold concentration increase, again in macrophages[66, 71].

BCG invasion and intracellular mycobacteria killing

The macrophage is an important site of replication and survival of *M. tuberculosis*.[7-9] Using *Mycobacterium bovis* Bacilli Calmette Guerin (BCG), intracellular killing assays were performed to assess the efficacy of synthesised P(ManAm)-*co*-P(DAAm-*hydrazone*-INH)-*co*-P(DPAEMA) particles. These were performed against the controls of free isoniazid at 7.2 μg mL^{-1}, Poly(Ethylene Glycol) Acrylate (PEGA) coated particles with cleavable isoniazid, mannose coated particles with no isoniazid and mannose coated particles with non-cleavable isoniazid: (P(PEGA)-*co*-P(DAAm-*hydrazone*-INH)-*co*-P(DPAEMA), P(ManAm)-*co*-P(DPAEMA), and P(ManAm)-*co*-P(*urea*-INH)-*co*-P(DPAEMA) respectively. An isoniazid concentration of 7.2 μg mL^{-1} was used as this is equivalent to the concentration of particle bound isoniazid at experimental concentration, and lies within the normal therapeutic range in serum (4.3-8.1 μg mL^{-1})[95, 96].

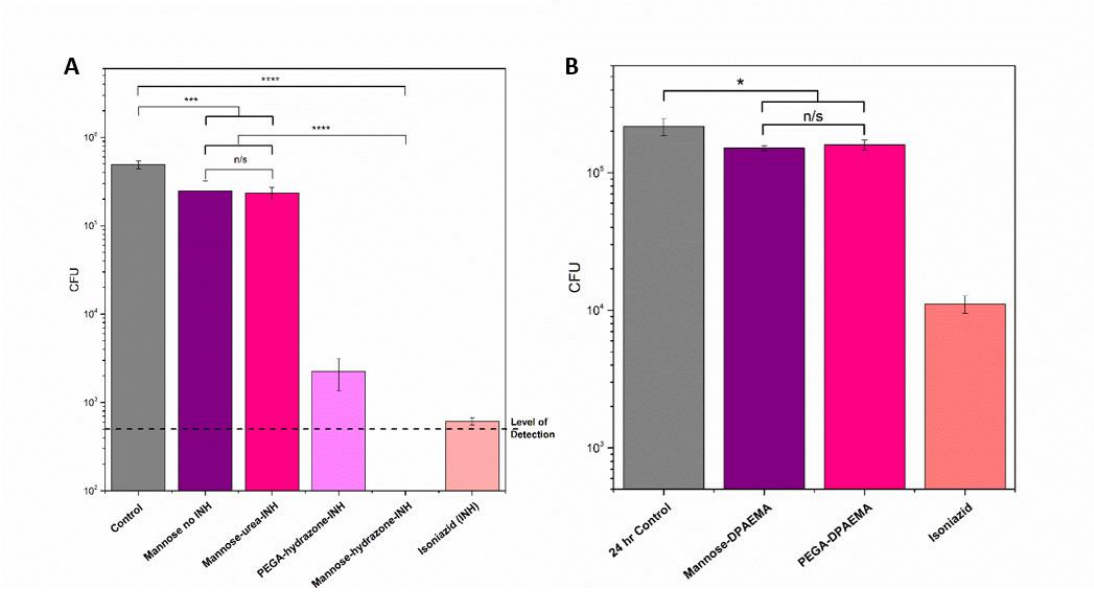

Figure 7: Intracellular BCG killing determined as number of viable bacteria as determined by colony forming units (CFU) after treatment, with positive controls of infected cells receiving no treatment at four and 24 hours. A) CFU counts comparing Mannose-(DAAm-*hydrazone*-INH)-DPAEMA particles against controls of PEGA-(DAAm-*hydrazone*-INH)-DPAEMA, Mannose-(DAAm-urea-INH)-DPAEMA and Mannose-DPAEMA particles, and equivalent free isoniazid. B) Colony counts comparing Mannose-DPAEMA particles to PEGA-DPAEMA particles and free isoniazid. Error bars show standard error, * = $p < 0.05$, ** = $p < 0.01$, *** = $p < 0.001$, **** = $p < 0.0001$ (Full statistical analysis Figures S14-15)

THP-1 macrophages were infected with *Mycobacterium bovis* BCG at a multiplicity of infection (MOI) of one, with extracellular BCG subsequently washed off and killed. Infected macrophages were incubated for 20 hours with treatment or control at 0.1 mg mL^{-1} polymer concentration or equivalent isoniazid concentration (7.2 μg mL^{-1}), following which intracellular bacterial counts were determined. Results were analysed for significance using an ANOVA with a post-hoc Tukey's range test. (Figure 7, S14)

The results showed that all treatments containing either free isoniazid or isoniazid bound by a cleavable hydrazone bond, exhibited significant bacterial killing compared to every other treatment group and positive controls. Delivery *via* a mannosylated particle improved the activity of the delivered dose of isoniazid, with P(ManAm)-*co*-P(DAAm-*hydrazone*-INH)-*co*-P(DPAEMA) being the only treatment showing complete bacterial eradication, as determined by colony counting. As the bacterial numbers obtained for PEGA-INH-DPAEA and INH treatments was close to the minimum level of detection, statistical significance could not be determined between them and the mannosylated particle. Nevertheless, this result was remarkable with the particulate systems retaining as a minimum, full antimicrobial activity, and achieving complete bacterial killing in 20 hours at a typical therapeutic serum concentration.[91, 95, 96] Similar studies, such as that from Horvati *et al*. used a similar analytical method and found that isoniazid conjugated poly(lactic-*co*-glycolic acid) (PLGA) particles, whilst having a greater antimicrobial effect than free isoniazid, still showed 50-100 bacterial colonies per well after three days treatment time[97].

Treatments without isoniazid, or where isoniazid had been introduced *via* a non-cleavable linker: P(ManAm)-*co*-P(DPAEMA) and P(ManAm)-*co*-P(*urea*-INH)-*co*-P(DPAEMA), showed a far reduced antimicrobial activity, with no statistical difference between the two treatments. This suggests that for the isoniazid to be active it must first be released from the polymer, and further indicates that the responsive systems were effectively releasing isoniazid. However, both control particles showed statistically significant antimicrobial activity compared to the 24 hours untreated control. It was not clear though if this activity was an

immunological response to the mannose present, or antimicrobial activity of the DPAEMA component that has recently been reported[98-101]. The most relevant of these reports being that of Phillips *et al.* who showed that poly(dimethylaminoethyl methacrylate) was active against *Mycobacterium smegmatis*, a bacterium of the same family as tuberculosis and BCG, but faster growing[102]. This study was limited to extracellular bacteria in MIC testing, interestingly, further work from the same group has revealed the antimicrobial effect of a polycation against *M. smegmatis* is bacteriostatic and not membrane lysing[103].

To determine the cause of the activity in this case, intracellular bacterial killing assays were performed with the P(ManAm)-*co*-P(DPAEMA) particle against controls of P(PEGA)-*co*-P(DPAEMA) and isoniazid (Figure 7, Table 1). Again, isoniazid showed good antimicrobial activity, with significantly reduced CFU counts against all other treatment groups and controls, validating the experiment. Both mannose and PEG coated particles showed limited, but statistically significant antimicrobial activity when compared to the 24-hour positive control, but showed no statistical difference to each other. Positive polymers are known to exhibit antimicrobial activity hence, protonation of the tertiary amine on DPAEMA in the acidic environment of the phagolysosome may be responsible for the activity seen[104]. This also suggests potential co-localisation within the macrophage between the polymer and bacteria.

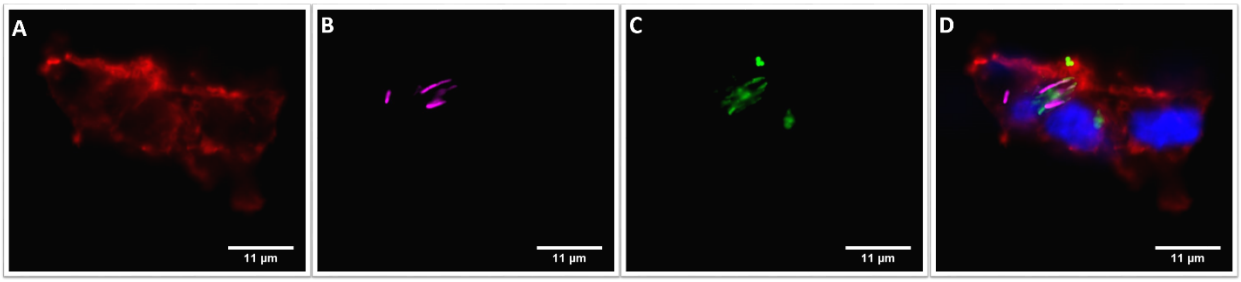

Figure 8: Confocal microscopy showing presence of investigative ManAm-DPAEMA-Cy3Am particle and BCG in close proximity. A) DyLight 650 phalloidin stained actin- red, B) eGFP BCG- magenta, C) ManAm-DPAEMA-Cy3Am particles- Green and D) Composite of images A-C with DAPI stained nucleus- blue. Images taken four hours post infection.

Particle-bacteria co-localisation confocal microscopy

To study intracellular co-localisation between particles and bacteria, THP-1 macrophages were infected with eGFP fluorescent BCG and treated with a fluorescent P(ManAm)-*co*-P(DPAEMA)-*co*-P(Cy3Am) particle, bearing no isoniazid so as not to eradicate BCG. Bacteria are visible in close vicinity to the particles (Figure 8). This would suggest that these are present in the same compartment and that there is the potential for the now positively charged polymer to directly interact with BCG intracellularly, providing a plausible explanation for antimicrobial activity.

The limited nature of the co-localised fluorescence, together with the likely bacteriostatic antimicrobial mechanism would further explain the very modest antimicrobial activity that the particles exhibit[103]. Where there is fluorescence from polymer and bacteria, the polymer fluorescence can in some cases be seen to be diffuse, and not clearly punctuated. A lack of punctuation could suggest that the particles are not compartmentalised in the cell and are escaping from the endocytic pathway compartment, which is likely to be a lysosome. Lysosomal escape would match with previous findings that nanoparticles and mycobacteria are found in different compartments of the macrophage, the phagosome and phagolysosome respectively. The tertiary amine also provides a mechanism by which escape may occur, with its buffering capacity potentially triggering the “proton sponge” effect causing phagolysosome rupture[105]. This provides a reasonable, but not conclusive explanation for interaction between

bacteria and polymer, and thus the displayed antimicrobial activity of the particles not bearing isoniazid.

Conclusion

Current therapy for TB infection requires long treatment times, and suffers from poor penetration to mycobacterium containing niches such as the macrophage.

The current work describes the synthesis of a novel antibiotic prodrug monomer, utilising the hydrazine group of isoniazid to form a hydrazone bond with the ketone present on diacetone acrylamide. This monomer was shown to be suitable for emulsion polymerisation. The hydrazone linker was demonstrated to be cleavable by a biologically relevant drop in pH from 7 to 5, yielding the active isoniazid compound. This monomer was co-polymerised with mannopyran-1-oxythyl acrylamide and DPAEMA in a free radical surfactant free emulsion polymerisation. Clinically relevant, dual pH responsive nanoparticles with diameters of *c.* 200 nm were synthesised, breaking apart and releasing the covalently bound isoniazid at pH 5 in PBS. Fluorescence uptake studies showed preferential endocytosis of mannosylated particles *via* sugar-lectin interactions, over a PEGylated control.

These particles were subsequently shown to be effective at killing intracellular *M. bovis* BCG bacteria in THP-1 macrophages, releasing their isoniazid cargo and exhibiting at least equivalent activity to free isoniazid in the artificial environment of a well plate, with P(ManAm)-*co*-P(DAAm-*hydrazone*-INH)-*co*-P(DPAEMA) particles being the only treatment to show complete bacterial eradication. This improved activity is hypothesised to be due to the increased cellular uptake of mannose coated particles, causing a higher intracellular isoniazid concentration compared to the controls. Furthermore, limited antimicrobial activity of the DPAEMA component of the particle was demonstrated, potentially contributing to the enhanced antimicrobial activity of the P(ManAm)-*co*-P(DAAm-*hydrazone*-INH)-*co*-P(DPAEMA) particle.

Taken together these results show that *in vitro,* such macrophage-targeted particles increase intracellular isoniazid concentration, showing an increased antimicrobial activity against intracellular mycobacteria, and leave the possibility for an enhanced effect *in vivo* to be studied.

Acknowledgements

The authors acknowledge funding from the Warwick-Wellcome Trust Translational Partnership Award.

Methods

Materials

Magnesium sulphate, isoniazid (≥ 99%), diacetone acrylamide (99%), poly(ethylene glycol) methyl ether acrylate (PEGA, average M_n= 480 g mol-1), 2-(diisopropylamino) ethyl methacrylate (97 %), acryloyl chloride (97%), 2-isocyanatoethyl methacrylate (98%), paraformaldehyde powder (95%), sodium hydroxide (≥ 97%), N-methylmorpholine (99%) phorbol myristate acetate (PMA, ≥ 99%), trifluoro acetic acid (>98%), Middlebrook 7H10 agar base, Middlebrook 7H10 broth base, glycerol (≥ 99%), hygromycin B from *Streptomyces hygroscopius*, amikacin (European pharmacopoeial standard), phenazine methosulfate (PMS)

(≥ 90%) and 2,3-Bis(2-methoxy-4-nitro-5-sulfophenyl)-2H-tetrazolium-5-carboxanilide inner salt (XTT) were purchased from Sigma-Aldrich and used as received except for all monomers that were passed through basic aluminium oxide to remove inhibitor. Thermal initiator VA-044 2,2'-Azobis[2-(2-imidazolin-2-yl)propane] dihydrochloride was purchased from Alpha Laboratories, Cyanine3 amine (95%) (Lumiprobe), Middlebrook OADC growth supplement (Agar Scientific), RPMI 1640 Medium, GlutaMAX™ Supplement, DMEM, Hoechst 33342 and fetal bovine serum (FBS) (ThermoFisher), Phalloidin DyLight 650 Phalloidin (300 unit) (New England Bioloabs), ProLong Gold Antifade Reagent with DAPI (Vector Laboratories), super smooth silicon wafers, adhesive copper tape were purchased from Agar Scientific and LabTek II 4-well microscopy culture slides were purchased from Thermo Scientific and all were used as purchased.

THP-1 (ATCC® TIB-202™), A549 (ATCC® CCL-185™), *Mycobacterium bovis* Karlson and Lessel (ATCC® 35737™), eGFP BCG was a kind gift from Dr Apoorva Bhatt, University of of Birmingham.

NMR spectroscopy

^{1}H NMR spectra were recorded on a Bruker DPX-300 spectrometer using deuterated solvent (materials section). Each sample was run with a decay time of 2 s with 16 repeats.

Mass spectrometry

ESI mass spectrometry measurements were performed using an Agilent 6130B single quad in methanol as a solvent in positive mode.

Melting point

Melting point temperatures were determined using a Stuart SMP10 digital melting point apparatus with a small amount of monomer placed into capillary tubing and repeated in triplicate, the average of all three readings reported in all cases.

Dynamic light scattering

Size measurements were carried out using a Malvern Zetasizer Nano-ZS at 25°C with a 4 mW He-Ne 633 nm laser at a scattering angle of 173° (back scattering). Measurements were taken assuming the refractive index of di-isopropyl aminoethyl methacrylate. Pdi values were calculated using Equation 1. Measurements of ζ-potential were modelled with the Smoluchowski theory. Samples for DLS and ζ-potential measurements were prepared by dilution of 15 µL of concentrated latex into 1.5 mL of neutral TRIS buffer.

$$\text{Pdi} = \frac{\sigma^2}{d^2}$$

Equation 1: Equation to calculate Pdi from standard deviation (σ), and diameter (d).

Scanning electron microscopy

SEM analysis was performed to determine the size and morphology of fluorescent particles as the fluorophore absorbed the laser used in DLS. Samples were prepared by diluting raw latex by a factor of 500 in previously filtered deionised water. A 5 µL drop of this diluted sample was then spotted onto a super smooth silicon wafer and left to dry for 12 hours in a laminar flow cabinet to ensure no sample contamination. The particles were visualised using a Zeiss Gemini SEM field emission scanning electron microscope at an accelerating voltage of 5 keV.

Particle size and standard deviation was determined by taking an average of 20 particle diameters using Image J software, Pdi was determined using Equation 1.

High performance liquid chromatography (HPLC)

HPLC samples were prepared by centrifuging the latex using an Eppendorf MiniSpin5452 at 13500 rpm for five minutes. The supernatant was aspirated off and filtered using a 0.2 μM PVC syringe filter. The filtered sample was then diluted by a factor of 100 into HPLC water eluent (0.05 TFA) at an injection volume of 100 μL. Chromatograms were obtained using an Agilent 1260 Infinity series equipped with an Agilent 1260 variable wavelength detector. The HPLC was fitted with a Phenomenex Luna® C18 (250 × 4.6 mm) with 5 μm packing (100 Å) column. Mobile phase A: water (+0.05 % TFA), mobile phase B: methanol (+0.05 % TFA). The gradient used for HPLC analysis was increased from 5% to 95 % B in 30 minutes. Detection for isoniazid release was achieved *via* monitoring at 270 nm. To detect Cy3 or Cy3Am the same procedure was carried out, with monitoring of fluorescence at excitation/emission wavelengths of 554/565 nm.

Isoniazid-diacetone acrylamide hydrazone, pH responsive monomer ((E)-N-(4-(2-isonicotinoylhydrazineylidene)-2-methylpentan-2-yl) acrylamide) synthesis

Isoniazid (5 g, 0.0365 mol, 1 eq.) and diacetone acrylamide (6.16 g, 0.0365 mol, 1 eq.) were dissolved in anhydrous methanol to a volume of 250 mL in a 500 mL round bottomed flask charged with a magnetic follower. Anhydrous magnesium sulphate (5g, 0.02 mol) was suspended in the reaction mixture to absorb water released by the condensation reaction, pushing the reaction equilibrium to the product. The flask was sealed with a rubber septum and left to stir at room temperature for 16 hours. The magnesium sulphate was then removed *via* Buchner filtration and methanol removed under vacuum using a rotary evaporator leaving behind a clear gel like solid, confirmed as the pure product by ^{1}H NMR spectroscopy, mass spectrometry and elemental analysis. (Figure S1)

MS m/z = 310.7 $[M+Na]^+$ (MS_{th}: 311.06): ^{1}H NMR (300 MHz, D_2O) δ 8.63 (t, *J* = 7.1 Hz, 2H), 7.69 (dd, *J* = 18.0, 5.9 Hz, 2H), 6.31 – 5.96 (m, 2H), 5.67 (dd, *J* = 28.4, 13.5 Hz, 1H), 2.92 (d, *J* = 67.0 Hz, 2H), 2.02 (d, *J* = 45.2 Hz, 3H), 1.43 – 1.27 (m, 6H): Melting point = 82°C

Isoniazid-diacetone acrylamide urea linked non-responsive monomer (2-(2-isonicotinoylhydrazine-1-carboxamido)ethyl methacrylate) synthesis

Isoniazid (804 mg, $5.86x10^{-3}$ mol, 1 eq.) and 2-icocyanatoethyl methacrylate (1g, $6.45x10^{-3}$ mol, 1.1 eq.) were dissolved in 50 mL of anhydrous methanol in a 100 mL round bottomed flask, charged with a magnetic follower. The flask was sealed with a rubber septum and left to stir. After four hours the product precipitated out of solution as a white powder. After cooling the reaction mixture to 8°C, full precipitation occurred and the precipitate was recovered by Buchner filtration using filter paper with pore size 11 μm. The powder was recrystallised using methanol as a solvent and confirmed as the product using ^{1}H NMR spectroscopy, mass spectrometry and elemental analysis. (Figure S2)

MS: *m/z* = 315.2 $[M+Na]^+$ (MS_{th}: 315.11): ^{1}H NMR (300 MHz, DMSO) δ 10.44 (s, 1H), 8.75 (d, *J* = 5.7 Hz, 2H), 8.11 (s, 1H), 7.79 (d, *J* = 5.7 Hz, 2H), 6.74 (t, *J* = 4.9 Hz, 1H), 6.06 (s, 1H), 5.67 (s, 1H), 4.08 (t, *J* = 5.7 Hz, 2H), 2.50 (s, 4H), 1.88 (s, 3H): Melting point =168°C

Cyanine 3 acrylamide synthesis

Cyanine 3 amine (5 mg, 7.965 mmol, 1 eq.), acryloyl chloride (0.793 mg, 8.76 mmol, 1.1 eq.) and N-methylmorpholine (NMM, 2.42 mg, 23.9 mmol, 3 eq.) were dissolved in 10 mL of

chloroform in a 20 mL glass vial charged with a magnetic follower. The vial was sealed with a rubber septum and moved into a cold room to react at 8°C for six hours. The chloroform solvent and NMM was then removed under vacuum using a rotary evaporator, leaving a red crystalline powder. Due to the low mass of reactants, no purification or ^{1}H NMR spectroscopy was performed, the product was confirmed using high resolution mass spectrometry and HPLC, showing only the shifted monomer peak in HPLC and m/z in mass spectrometry. (Figure S3)

MS: m/z = 609.4 $[Mw]^{+}$ (MS_{th}: 609.42).

General particle synthesis method

Nanoparticles of varying composition were synthesised by varying the monomers in the reaction mixture. The general method by which nanoparticles were prepared is represented by the following, using P(ManAm)-*co*-P(DAAm-*hydrazone*-INH)-*co*-P(DPAEMA) as an example. 50 mg VA-044 (1.6 x 10^{-4} mol) was added to 10 mL of deionised water to produce a 5 mg mL^{-1} initiator stock solution. 13 mg of mannopyran-1-oxyethyl acrylamide (4.67 x10^{-5} M) and 13.5 mg (4.69 x10^{-5} M) DAAm-*hydrazone*-INH was weighed into a tared 7.5 mL glass vial, 1.68 mL of deionised water was then added into the glass vial using an auto-pipette, to which 0.3 mL of the previously described stock solution of VA-044 was added. The glass vial was then charged with a 1 cm magnetic stirrer bar, sealed with a size 21 septum and purged of oxygen by bubbling nitrogen through the solution for 10 minutes. In a separate 20 mL glass vial, sealed with a size 33 septum, DPAEMA was purged of oxygen by bubbling nitrogen through the liquid monomer for 10 minutes. After both solutions had been purged, 18 mg of DPAEMA (8.4x10^{-5} moles, 0.02 mL)) was transferred into the 7.5 mL glass vial using a gas tight Hamilton syringe that had been purged of oxygen. The 7.5 mL vial was placed into an oil bath set to 50°C and stirred at a rate of 800 rpm for three hours. After approximately 5-10 minutes the reaction mixture turned a uniform white milky colour as the particles nucleated and the polymerisation proceeded. At the end of three hours the reaction was quenched by removing the vial from the oil bath and exposing it to oxygen by removing the septum. The resulting latex was analysed by DLS to determine particle size and dispersity (diameter = 212 nm, Pdi = 0.1) (Figure S4)

Cell culture

A549 (lung epithelial carcinoma) cells were grown in Dulbecco's modified Eagle's medium (DMEM) supplemented with 10% (v/v) fetal bovine serum (FBS) and 2 mM of glutamine and pen/strep at 37°C in a sterile, humid 5% CO_2 environment. Human Leukaemia (THP)-1 monocyte cells were grown in Roswell Park Memorial Institute (RPMI) 1640 GlutaMAX Medium supplemented with 20% (v/v) FBS at 37°C in a sterile, humid 5% CO2 environment.

2,3-Bis-(2-Methoxy-4-Nitro-5-Sulfophenyl)-2H-Tetrazolium-5-Carboxanilide (XTT) cell viability assay

THP-1 monocytes were seeded at a density of 2.5x10^{5} cells per mL into a 96 well plate in RPMI Glutamax media supplemented with 20% FBS and 100 ng mL^{-1} PMA in order to differentiate the cells to adherent macrophages and incubated for 72 hours at 37°C. Or; A549 cells were seeded at a density of 5x10^{5} cells per mL of DMEM (supplemented with 10% FBS, 1% glutamine and 1% pen/strep) into a 96 well plate and incubated for 24 hours at 37°C. In both cases after incubation, fresh media was replaced in all of the wells. The cells were then incubated with serial dilutions of the particles at 0.1 μg mL^{-1}, 1 μg mL^{-1}, 10 μg mL^{-1}, 0.1 mg mL^{-1}, 0.5 mg mL^{-1} and 2 mg mL^{-1} for 72 hours. To determine the cell viability a standard XTT assay was used.[106] The cell media was replaced with 100 μL fresh media and 100 μL of a 0.0083 mM phenazine methosulfate (PMS)/ 0.33 mg mL^{-1} XTT solution in media and left to

incubate at 37°C for 24 hours. Each well then had its absorbance recorded using a BioTek Cytation3 plate reader at 450 nm and 650 nm (background). The relative absorbance compared to a control of healthy cells as 100% cell viability was recorded and used to show the percentage cell viability in each case. The experiments were carried out with three technical replicates in triplicate.

Macrophage particle uptake assay

THP-1 cells were seeded at a density of $2.5x10^5$ cells per mL into a 96 well plate in RPMI Glutamax media supplemented with 20% FBS, and 100 ng mL^{-1} PMA in order to differentiate the cells to adherent THP macrophages and incubated for 72 hours at 37°C to form adherent monolayers. The media was then replaced and cells were inoculated for either 24, six or two hours with either PEG or mannose coated fluorescent particles at a concentration of 0.1 mg mL^{-1}. At 23 hours and 30 minutes incubation time, 10 µL of a 50 µg mL^{-1} Hoescht 33342 in PBS stock solution was added to the wells and incubated at 37°C for a further 30 minutes to stain the nucleus of the cells. The media was then removed and any extra cellular particles removed by with PBS three times. The cells were incubated in phenol red free media and placed into a BioTek Citation3 plate reader, to determine the level of fluorescence in each cell. The nucleus of each cell was imaged as a reference, set at absorption/emission detection of 377/477 nm for Hoechst 33342, and the fluorescence of cyanine 3 labelled particles at an absoption/emission of 531/593 nm. From the nucleus a representative cell size cut off of 13 µm was applied and using a rolling ball algorithm for background calculation, particle fluorescence per cell over hundreds of cells was determined and an average taken. This was repeated with three technical replicates in duplicate. To ensure any difference in fluorescence was due to changes in uptake, and not differing fluorescence intensity, a fluorescence calibration for both PEG and mannose particles was then produced. This was determined by serially diluting a 1 mg mL^{-1} stock of each particle by half repeatedly 15 times and taking a fluorescence reading of each, this was repeated in triplicate. The difference in relative fluorescence intensities was then determined by comparing the extinction co-efficient for each calibration. The relative fluorescence for both particles was found to be at a ratio of 1:0.97, and as such, within error of each other, however to ensure that differing fluorescence did not contribute to any observed differences in uptake, the readings for PEG particles were multiplied by 0.97 (Figure 5).

Confocal microscopy cell uptake

THP-1 derived macrophage cells were cultured on LabTek II 4-well microscopy culture slides as described for a 96 well plate in section "Macrophage Particle Uptake Assay". After incubating with fluorescent mannose particles for two, six and 24 hours at 0.1 mg mL^{-1} the cells were washed three times with PBS and fixed by incubation with 1 mL of a cooled 4% PFA solution at room temperature for ten minutes. This was washed three times with PBS. Cells were permeabilized in 1 mL of a 1% saponin, 0.5% Triton X-100 solution in PBS for 20 minutes at room temperature, then blocked with 0.5 mL of a 3% bovine serum albumin (BSA) solution in PBS for 30 minutes at room temperature. Culture slides were then washed with 0.5 mL of 1% BSA in PBS. F-actin was then stained by adding 0.2 mL of a 2.5 µg mL^{-1} solution of phalloidin 650 in 1% BSA for 40 minutes in the dark at room temperature. Chamber slides were washed with 1 mL of PBS three times and chambers removed from the culture slides. A cover slip was then secured using 10 µL of DAPI mounting medium per well, also staining the nuclei of the cells. Slides were then kept in the dark between 2-8 °C until imaging. Confocal images were taken on a Zeiss 880 at 37 °C using a 40x objective lens and sequential scanning for each channel. Excitation/emission used for imaging was as follows: nucleus DAPI 405/410-480 nm, Cy3 particles 561/567-620 nm, DyLight 650 phalloidin 633/639-759 nm. Images were overlaid and processed using Image-J software.

BCG invasion and intracellular killing assays

Intracellular infection was performed on THP-1 derived macrophages. Cells were seeded at a density of $2.5x10^5$ cells per mL into a 24 well plate in RPMI Glutamax media supplemented with 20% FBS, and 100 ng mL^{-1} PMA in order to differentiate the cells to adherent macrophages and incubated for 72 hours at 37°C. A single colony of BCG bacteria was inoculated in Middlebrook 7H10 broth supplemented with 10% (v/v) OADC enrichment. The inoculum was grown to an OD_{600}=0.8,and diluted ten-fold into cell culture medium (RPMI GlutMAX + 20% FBS) and incubated with macrophages for three hours at 37 °C giving an MOI of 1:1. Extracellular bacteria were then removed with PBS three times and the macrophages incubated with 1 mL solution of 200 ng mL^{-1} amikacin in media for one hour to ensure no viable extracellular BCG. Cells were then further washed with 1 mL of PBS twice. These cells were then either lysed by incubating in cold water for 5 minutes at RT followed by vigorous pipetting (4 hour time point) or incubated further for 20 hrs. Cell lysates were immediately diluted by a factor of ten into warm PBS twice. 20 µL of each dilution was pipetted onto Middlebrook 7H10 ADC agar petri dishes and incubated at 37 °C for 14-21 days to allow bacterial growth. After two weeks CFU counts for all dilutions were performed and the total number of CFU's per well determined using Equation 2.

$$CFU_{Total} = CFU_{Counted} \times (50 \times Dilution\ Factor)$$

Equation 2. Calculation performed to determine viable number of colony forming units (CFU) using dilute 20 µL sample from a 1 mL well

Confocal microscopy of particle/bacteria co-localisation

THP-1 derived M0 macrophage cells were cultures on LabTek II 4-well microscopy culture slides as described for 24 well plates in the section "Intracellular BCG Killing Assays", and fixed as described in "Confocal Microscopy, Cell Uptake". Excitation/emission of eGFP BCG used for imaging was 490/500-540 nm. Images were overlaid and processed using Image-J software.

Statistical analysis

All analyses were performed using IBM SPSS Statistics 24. The test used for comparison of the means of particle uptake at 2, 6 and 24 hours for PEG versus mannose coated particles was a Student's T-test. Normality of distribution was verified with a Kolmogorov-Smirnov non-parametrical test. The test performed to compare all CFU count data after intracellular BCG killing was a one-way ANOVA test with a Tukey post-hoc analysis. The assumptions for the tests were: normality of distribution (verified with a Kolmogorov-Smirnov non-parametrical test), homogeneity of variances (evaluated using a Levene test). Analysis was performed on two or three biological repeats performed with three technical repeats in all cases.

References

1. García-Basteiro, A. L.; Brew, J.; Williams, B.; Borgdorff, M.; Cobelens, F., What is the true tuberculosis mortality burden? Differences in estimates by the World Health Organization and the Global Burden of Disease study. *International Journal of Epidemiology* **2018**.
2. Lee, J. Y., Diagnosis and treatment of extrapulmonary tuberculosis. *Tuberculosis Respiratory Diseases* **2015,** *78* (2), 47-55.
3. Glaziou, P.; Floyd, K.; Raviglione, M. C. In *Global Epidemiology of Tuberculosis*, Seminars in Respiratory and Critical Care Medicine, Thieme Medical Publishers: 2018; pp 271-285.

4. Shishido, Y.; Mitarai, S.; Otomo, K.; Seki, M.; Sato, A.; Yano, I.; Koyama, A.; Hattori, T., Anti-tuberculosis drug susceptibility testing of Mycobacterium bovis BCG Tokyo strain. *The International Journal of Tuberculosis Lung Disease* **2007,** *11* (12), 1334-1338.
5. Kolibab, K.; Derrick, S. C.; Morris, S. L., Sensitivity to isoniazid of Mycobacterium bovis BCG strains and BCG disseminated disease isolates. *Journal of Clinical Microbiology* **2011,** *49* (6), 2380-2381.
6. Gilpin, C.; Korobitsyn, A.; Migliori, G. B.; Raviglione, M. C.; Weyer, K., The World Health Organization standards for tuberculosis care and management. Eur Respiratory Soc: 2018.
7. Madigan, C. A.; Cameron, J.; Ramakrishnan, L., A zebrafish model of Mycobacterium leprae granulomatous infection. *The Journal of Infectious Diseases* **2017,** *216* (6), 776-779.
8. Conrad, W. H.; Osman, M. M.; Shanahan, J. K.; Chu, F.; Takaki, K. K.; Cameron, J.; Hopkinson-Woolley, D.; Brosch, R.; Ramakrishnan, L., Mycobacterial ESX-1 secretion system mediates host cell lysis through bacterium contact-dependent gross membrane disruptions. *Proceedings of the National Academy of Sciences* **2017,** *114* (6), 1371-1376.
9. Cambier, C.; O'Leary, S. M.; O'Sullivan, M. P.; Keane, J.; Ramakrishnan, L., Phenolic glycolipid facilitates mycobacterial escape from microbicidal tissue-resident macrophages. *Immunity* **2017,** *47* (3), 552-565. e4.
10. Hayashi, D.; Takii, T.; Mukai, T.; Makino, M.; Yasuda, E.; Horita, Y.; Yamamoto, R.; Fujiwara, A.; Kanai, K.; Kondo, M., Biochemical characteristics among Mycobacterium bovis BCG substrains. *FEMS Microbiology Letters* **2010,** *306* (2), 103-109.
11. Gill, W. P.; Harik, N. S.; Whiddon, M. R.; Liao, R. P.; Mittler, J. E.; Sherman, D. R., A replication clock for Mycobacterium tuberculosis. *Nature Medicine* **2009,** *15* (2), 211.
12. Gebremariam, M. K.; Bjune, G. A.; Frich, J. C., Barriers and facilitators of adherence to TB treatment in patients on concomitant TB and HIV treatment: a qualitative study. *BMC Public Health* **2010,** *10* (1), 651.
13. Kaona, F. A.; Tuba, M.; Siziya, S.; Sikaona, L., An assessment of factors contributing to treatment adherence and knowledge of TB transmission among patients on TB treatment. *BMC Public Health* **2004,** *4* (1), 68.
14. Diacon, A. H.; Dawson, R.; von Groote-Bidlingmaier, F.; Symons, G.; Venter, A.; Donald, P. R.; van Niekerk, C.; Everitt, D.; Winter, H.; Becker, P., 14-day bactericidal activity of PA-824, bedaquiline, pyrazinamide, and moxifloxacin combinations: a randomised trial. *The Lancet* **2012,** *380* (9846), 986-993.
15. Diacon, A.; Donald, P.; Pym, A.; Grobusch, M.; Patientia, R.; Mahanyele, R.; Bantubani, N.; Narasimooloo, R.; De Marez, T.; Van Heeswijk, R., Randomized pilot trial of eight weeks of bedaquiline (TMC207) treatment for multidrug-resistant tuberculosis: long-term outcome, tolerability, and effect on emergence of drug resistance. *Antimicrobial Agents Chemotherapy* **2012,** *56* (6), 3271-3276.
16. Diacon, A. H.; Pym, A.; Grobusch, M. P.; de Los Rios, J. M.; Gotuzzo, E.; Vasilyeva, I.; Leimane, V.; Andries, K.; Bakare, N.; De Marez, T., Multidrug-resistant tuberculosis and culture conversion with bedaquiline. *New England Journal of Medicine* **2014,** *371* (8), 723-732.
17. Raju, R. M.; Unnikrishnan, M.; Rubin, D. H.; Krishnamoorthy, V.; Kandror, O.; Akopian, T. N.; Goldberg, A. L.; Rubin, E. J., Mycobacterium tuberculosis ClpP1 and ClpP2 function together in protein degradation and are required for viability in vitro and during infection. *PLoS Pathogens* **2012,** *8* (2), e1002511.
18. Gelperina, S.; Kisich, K.; Iseman, M. D.; Heifets, L., The potential advantages of nanoparticle drug delivery systems in chemotherapy of tuberculosis. *American Journal of Respiratory Critical Care Medicine* **2005,** *172* (12), 1487-1490.

19. Mignani, S.; Tripathi, R.; Chen, L.; Caminade, A.-M.; Shi, X.; Majoral, J.-P., New Ways to Treat Tuberculosis Using Dendrimers as Nanocarriers. *Pharmaceutics* **2018,** *10* (3), 105.
20. Su, F.-Y.; Chen, J.; Son, H.-N.; Kelly, A. M.; Convertine, A. J.; West, T. E.; Skerrett, S. J.; Ratner, D. M.; Stayton, P. S., Polymer-augmented liposomes enhancing antibiotic delivery against intracellular infections. *Biomaterials Science* **2018**.
21. Soppimath, K. S.; Aminabhavi, T. M.; Kulkarni, A. R.; Rudzinski, W. E., Biodegradable polymeric nanoparticles as drug delivery devices. *Journal of Controlled Release* **2001,** *70* (1-2), 1-20.
22. Kumari, A.; Yadav, S. K.; Yadav, S. C., Biodegradable polymeric nanoparticles based drug delivery systems. *Colloids Surfaces B: Biointerfaces* **2010,** *75* (1), 1-18.
23. Cho, K.; Wang, X.; Nie, S.; Shin, D. M., Therapeutic nanoparticles for drug delivery in cancer. *Clinical Cancer Research* **2008,** *14* (5), 1310-1316.
24. Singh, R.; Lillard Jr, J. W., Nanoparticle-based targeted drug delivery. *Experimental Molecular Pathology* **2009,** *86* (3), 215-223.
25. Fitch, R. M., *Polymer colloids*. Academic Press: 1997.
26. Tadros, T. F., *Handbook of Colloid and Interface Science: Industrial Applications*. Walter de Gruyter GmbH & Co KG: 2017; Vol. 3.
27. Chern, C.; Lin, S.; Chang, S.; Lin, J.; Lin, Y., Effect of initiator on styrene emulsion polymerisation stabilised by mixed SDS/NP-40 surfactants. *Polymer* **1998,** *39* (11), 2281-2289.
28. Robertson, J. D.; Rizzello, L.; Avila-Olias, M.; Gaitzsch, J.; Contini, C.; Magoń, M. S.; Renshaw, S. A.; Battaglia, G., Purification of Nanoparticles by Size and Shape. *Scientific Reports* **2016,** *6*, 27494.
29. Luo, Z.; Zou, C.; Syed, S.; Syarbaini, L. A.; Chen, G., Highly monodisperse chemically reactive sub-micrometer particles: polymer colloidal photonic crystals. *Colloid and Polymer Science* **2012,** *290* (2), 141-150.
30. Mahapatro, A.; Singh, D. K., Biodegradable nanoparticles are excellent vehicle for site directed in-vivo delivery of drugs and vaccines. *Journal of Nanobiotechnology* **2011,** *9* (1), 55.
31. Siauw, M.; Hawkett, B. S.; Perrier, S., Short chain amphiphilic diblock co-oligomers via RAFT polymerization. *Journal of Polymer Science Part A: Polymer Chemistry* **2012,** *50* (1), 187-198.
32. Rieger, J.; Zhang, W.; Stoffelbach, F. o.; Charleux, B., Surfactant-free RAFT emulsion polymerization using poly (N, N-dimethylacrylamide) trithiocarbonate macromolecular chain transfer agents. *Macromolecules* **2010,** *43* (15), 6302-6310.
33. Prescott, S. W.; Ballard, M. J.; Rizzardo, E.; Gilbert, R. G., Successful use of RAFT techniques in seeded emulsion polymerization of styrene: living character, RAFT agent transport, and rate of polymerization. *Macromolecules* **2002,** *35* (14), 5417-5425.
34. Poon, C. K.; Tang, O.; Chen, X.-M.; Pham, B. T.; Gody, G.; Pollock, C. A.; Hawkett, B. S.; Perrier, S., Preparation of Inert Polystyrene Latex Particles as MicroRNA Delivery Vectors by Surfactant-Free RAFT Emulsion Polymerization. *Biomacromolecules* **2016,** *17* (3), 965-973.
35. Ferguson, C. J.; Hughes, R. J.; Nguyen, D.; Pham, B. T.; Gilbert, R. G.; Serelis, A. K.; Such, C. H.; Hawkett, B. S., Ab Initio Emulsion Polymerization by RAFT-Controlled Self-Assembly §. *Macromolecules* **2005,** *38* (6), 2191-2204.
36. Chiefari, J.; Chong, Y.; Ercole, F.; Krstina, J.; Jeffery, J.; Le, T. P.; Mayadunne, R. T.; Meijs, G. F.; Moad, C. L.; Moad, G., Living free-radical polymerization by reversible addition− fragmentation chain transfer: the RAFT process. *Macromolecules* **1998,** *31* (16), 5559-5562.
37. Boyer, C.; Bulmus, V.; Davis, T. P.; Ladmiral, V.; Liu, J.; Perrier, S., Bioapplications of RAFT polymerization. *Chemical Reviews* **2009,** *109* (11), 5402-5436.

38. Nurumbetov, G.; Engelis, N.; Godfrey, J.; Hand, R.; Anastasaki, A.; Simula, A.; Nikolaou, V.; Haddleton, D. M., Methacrylic block copolymers by sulfur free RAFT (SF RAFT) free radical emulsion polymerisation. *Polymer Chemistry* **2017,** *8* (6), 1084-1094.
39. Roe, C. P., Surface chemistry aspects of emulsion polymerization. *Industrial and Engineering Chemistry* **1968,** *60* (9), 20-33.
40. Goodall, A.; Wilkinson, M.; Hearn, J., Mechanism of emulsion polymerization of styrene in soap-free systems. *Journal of Polymer Science Part A: Polymer Chemistry* **1977,** *15* (9), 2193-2218.
41. Fan, X.; Liu, Y.; Jia, X.; Wang, S.; Li, C.; Zhang, B.; Zhang, H.; Zhang, Q., Regulating the size and molecular weight of polymeric particles by 1, 1-diphenylethene controlled soap-free emulsion polymerization. *RSC Advances* **2015,** *5* (115), 95183-95190.
42. Appel, J.; Akerboom, S.; Fokkink, R. G.; Sprakel, J., Facile One-Step Synthesis of Monodisperse Micron-Sized Latex Particles with Highly Carboxylated Surfaces. *Macromolecular Rapid Communications* **2013,** *34* (16), 1284-1288.
43. Egen, M.; Zentel, R., Surfactant-Free Emulsion Polymerization of Various Methacrylates: Towards Monodisperse Colloids for Polymer Opals. *Macromolecular Chemistry and Physics* **2004,** *205* (11), 1479-1488.
44. Tauer, K.; Deckwer, R.; Kühn, I.; Schellenberg, C., A comprehensive experimental study of surfactant-free emulsion polymerization of styrene. *Colloid and Polymer Science* **1999,** *277* (7), 607-626.
45. Rao, J. P.; Geckeler, K. E., Polymer nanoparticles: preparation techniques and size-control parameters. *Progress in Polymer Science* **2011,** *36* (7), 887-913.
46. Bao, J.; Zhang, A., Poly (methyl methacrylate) nanoparticles prepared through microwave emulsion polymerization. *Journal of Applied Polymer Science* **2004,** *93* (6), 2815-2820.
47. Thickett, S. C.; Gilbert, R. G., Emulsion polymerization: state of the art in kinetics and mechanisms. *Polymer* **2007,** *48* (24), 6965-6991.
48. Telford, A. M.; Pham, B. T.; Neto, C.; Hawkett, B. S., Micron-sized polystyrene particles by surfactant-free emulsion polymerization in air: Synthesis and mechanism. *Journal of Polymer Science Part A: Polymer Chemistry* **2013,** *51* (19), 3997-4002.
49. Peach, S., Coagulative nucleation in surfactant-free emulsion polymerization. *Macromolecules* **1998,** *31* (10), 3372-3373.
50. Feeney, P. J.; Napper, D. H.; Gilbert, R. G., Surfactant-free emulsion polymerizations: predictions of the coagulative nucleation theory. *Macromolecules* **1987,** *20* (11), 2922-2930.
51. Lunn, A. M.; Perrier, S., Synthesis of Sub-100 nm Glycosylated Nanoparticles via a One Step, Free Radical, and Surfactant Free Emulsion Polymerization. *Macromolecular Rapid Communications* **2018**, 1800122.
52. Rao, M.; Streur, T. L.; Aldwell, F. E.; Cook, G. M., Intracellular pH regulation by Mycobacterium smegmatis and Mycobacterium bovis BCG. *Microbiology* **2001,** *147* (4), 1017-1024.
53. Ohkuma, S.; Poole, B., Fluorescence probe measurement of the intralysosomal pH in living cells and the perturbation of pH by various agents. *Proceedings of the National Academy of Sciences* **1978,** *75* (7), 3327-3331.
54. Su, F.-Y.; Srinivasan, S.; Lee, B.; Chen, J.; Convertine, A. J.; West, T. E.; Ratner, D. M.; Skerrett, S. J.; Stayton, P. S., Macrophage-targeted drugamers with enzyme-cleavable linkers deliver high intracellular drug dosing and sustained drug pharmacokinetics against alveolar pulmonary infections. *Journal of Controlled Release* **2018,** *287*, 1-11.
55. Crisan, D. N.; Creese, O.; Ball, R.; Brioso, J. L.; Martyn, B.; Montenegro, J.; Fernandez-Trillo, F., Poly (acryloyl hydrazide), a versatile scaffold for the preparation of

functional polymers: synthesis and post-polymerisation modification. *Polymer Chemistry* **2017,** *8* (31), 4576-4584.
56. Prabaharan, M.; Grailer, J. J.; Pilla, S.; Steeber, D. A.; Gong, S., Amphiphilic multi-arm-block copolymer conjugated with doxorubicin via pH-sensitive hydrazone bond for tumor-targeted drug delivery. *Biomaterials* **2009,** *30* (29), 5757-5766.
57. Takeuchi, I.; Nobata, S.; Oiri, N.; Tomoda, K.; Makino, K., Biodistribution and excretion of colloidal gold nanoparticles after intravenous injection: Effects of particle size. *Bio-Medical Materials Engineering* **2017,** *28* (3), 315-323.
58. Madsen, J.; Madden, G.; Themistou, E.; Warren, N. J.; Armes, S. P., pH-Responsive diblock copolymers with two different fluorescent labels for simultaneous monitoring of micellar self-assembly and degree of protonation. *Polymer Chemistry* **2018,** *9* (21), 2964-2976.
59. Qiu, S.; Huang, H.; Dai, X. H.; Zhou, W.; Dong, C. M., Star-shaped polypeptide/glycopolymer biohybrids: Synthesis, self-assembly, biomolecular recognition, and controlled drug release behavior. *Journal of Polymer Science Part A: Polymer Chemistry* **2009,** *47* (8).
60. Boye, S.; Appelhans, D.; Boyko, V.; Zschoche, S.; Komber, H.; Friedel, P.; Formanek, P.; Janke, A.; Voit, B.; Lederer, A., pH-triggered aggregate shape of different generations lysine-dendronized maleimide copolymers with maltose shell. *Biomacromolecules* **2012,** *13* (12), 4222-4235.
61. Bae, Y.; Nishiyama, N.; Fukushima, S.; Koyama, H.; Yasuhiro, M.; Kataoka, K., Preparation and biological characterization of polymeric micelle drug carriers with intracellular pH-triggered drug release property: tumor permeability, controlled subcellular drug distribution, and enhanced in vivo antitumor efficacy. *Bioconjugate Chemistry* **2005,** *16* (1), 122-130.
62. Smith, A. E.; Xu, X.; McCormick, C. L., Stimuli-responsive amphiphilic (co) polymers via RAFT polymerization. *Progress in Polymer Science* **2010,** *35* (1-2), 45-93.
63. Yuan, W.; Yuan, J.; Zheng, S.; Hong, X., Synthesis, characterization, and controllable drug release of dendritic star-block copolymer by ring-opening polymerization and atom transfer radical polymerization. *Polymer* **2007,** *48* (9), 2585-2594.
64. Bütün, V.; Bennett, C. E.; Vamvakaki, M.; Lowe, A. B.; Billingham, N. C.; Armes, S. P., Selective betainisation of tertiary amine methacrylate blockcopolymers. *Journal of Materials Chemistry B* **1997,** *7* (9), 1693-1695.
65. Sun, X.; Jiang, G.; Wang, Y.; Xu, Y., Synthesis and drug release properties of novel pH-and temperature-sensitive copolymers based on a hyperbranched polyether core. *Colloid Polymer Science* **2011,** *289* (5-6), 677-684.
66. Chono, S.; Tanino, T.; Seki, T.; Morimoto, K., Efficient drug targeting to rat alveolar macrophages by pulmonary administration of ciprofloxacin incorporated into mannosylated liposomes for treatment of respiratory intracellular parasitic infections. *Journal of Controlled Release* **2008,** *127* (1), 50-58.
67. Wijagkanalan, W.; Kawakami, S.; Takenaga, M.; Igarashi, R.; Yamashita, F.; Hashida, M., Efficient targeting to alveolar macrophages by intratracheal administration of mannosylated liposomes in rats. *Journal of Controlled Release* **2008,** *125* (2), 121-130.
68. Chono, S.; Tanino, T.; Seki, T.; Morimoto, K., Uptake characteristics of liposomes by rat alveolar macrophages: influence of particle size and surface mannose modification. *Journal of Pharmacy Pharmacology* **2007,** *59* (1), 75-80.
69. Yilmaz, G.; Becer, C. R., Precision glycopolymers and their interactions with lectins. *European Polymer Journal* **2013,** *49* (10), 3046-3051.
70. Azad, A. K.; Rajaram, M. V.; Schlesinger, L. S., Exploitation of the macrophage mannose receptor (CD206) in infectious disease diagnostics and therapeutics. *Journal of Cytology Molecular Biology* **2014,** *1* (1).

71. Chono, S.; Tanino, T.; Seki, T.; Morimoto, K., Uptake characteristics of liposomes by rat alveolar macrophages: influence of particle size and surface mannose modification. *Journal of Pharmacy Pharmacology and Therapeutics* **2007,** *59* (1), 75-80.
72. Irache, J. M.; Salman, H. H.; Gamazo, C.; Espuelas, S., Mannose-targeted systems for the delivery of therapeutics. *Expert Opinion on Drug Delivery* **2008,** *5* (6), 703-724.
73. Azad, A. K.; Rajaram, M. V.; Schlesinger, L. S., Exploitation of the macrophage mannose receptor (CD206) in infectious disease diagnostics and therapeutics. *Journal of cytology & molecular biology* **2014,** *1* (1).
74. Taylor, M. E., Primary structure of the mannose receptor contains multiple motifs resembling carbohydrate-recognition domains. *The Journal of Biological Chemistry* **1990,** *265* (21), 12156-12162.
75. Ponader, D.; Maffre, P.; Aretz, J.; Pussak, D.; Ninnemann, N. M.; Schmidt, S.; Seeberger, P. H.; Rademacher, C.; Nienhaus, G. U.; Hartmann, L., Carbohydrate-lectin recognition of sequence-defined heteromultivalent glycooligomers. *Journal of the American Chemical Society* **2014,** *136* (5), 2008-2016.
76. Pieters, R. J., Maximising multivalency effects in protein–carbohydrate interactions. *Organic and Biomolecular Chemistry* **2009,** *7* (10), 2013-2025.
77. Gurnani, P.; Lunn, A. M.; Perrier, S., Synthesis of mannosylated and PEGylated nanoparticles via RAFT emulsion polymerisation, and investigation of particle-lectin aggregation using turbidimetric and DLS techniques. *Polymer* **2016,** *106*, 229-237.
78. He, C.; Hu, Y.; Yin, L.; Tang, C.; Yin, C., Effects of particle size and surface charge on cellular uptake and biodistribution of polymeric nanoparticles. *Biomaterials* **2010,** *31* (13), 3657-3666.
79. Shang, L.; Nienhaus, K.; Nienhaus, G. U., Engineered nanoparticles interacting with cells: size matters. *Journal of Nanobiotechnology* **2014,** *12* (1), 5.
80. Banik, N.; Hussain, A.; Ramteke, A.; Sharma, H. K.; Maji, T. K., Preparation and evaluation of the effect of particle size on the properties of chitosan-montmorillonite nanoparticles loaded with isoniazid. *RSC Advances* **2012,** *2* (28), 10519-10528.
81. Pandey, R.; Zahoor, A.; Sharma, S.; Khuller, G., Nanoparticle encapsulated antitubercular drugs as a potential oral drug delivery system against murine tuberculosis. *Tuberculosis* **2003,** *83* (6), 373-378.
82. Rani, S.; Gothwal, A.; Khan, I.; Pachouri, P. K.; Bhaskar, N.; Gupta, U. D.; Chauhan, D. S.; Gupta, U., Smartly Engineered PEGylated Di-Block Nanopolymeric Micelles: Duo Delivery of Isoniazid and Rifampicin Against Mycobacterium tuberculosis. *AAPS PharmSciTech* **2018,** *19* (7), 3237-3248.
83. Shen, S.; Wu, Y.; Liu, Y.; Wu, D., High drug-loading nanomedicines: progress, current status, and prospects. *International Journal of Nanomedicine* **2017,** *12*, 4085.
84. WHO; Organization, W. H., *Guidelines on the Management of Latent Tuberculosis Infection*. World Health Organization: 2015.
85. Hwang, A. A.; Lee, B. Y.; Clemens, D. L.; Dillon, B. J.; Zink, J. I.; Horwitz, M. A., pH-Responsive Isoniazid-Loaded Nanoparticles Markedly Improve Tuberculosis Treatment in Mice. *Small* **2015,** *11* (38), 5066-5078.
86. Nkanga, C. I.; Walker, R. B.; Krause, R. W., pH-Dependent release of isoniazid from isonicotinic acid (4-hydroxy-benzylidene)-hydrazide loaded liposomes. *Journal of Drug Delivery Science Technology* **2018,** *45*, 264-271.
87. Nkanga, C. I.; Krause, R. W. M., Conjugation of isoniazid to a zinc phthalocyanine via hydrazone linkage for pH-dependent liposomal controlled release. *Applied Nanoscience* **2018**, 1-11.

88. Xu, X.; Smith, A. E.; Kirkland, S. E.; McCormick, C. L., Aqueous RAFT synthesis of pH-responsive triblock copolymer mPEO− PAPMA− PDPAEMA and formation of shell cross-linked micelles. *Macromolecules* **2008,** *41* (22), 8429-8435.
89. Kakwere, H.; Perrier, S., Design of complex polymeric architectures and nanostructured materials/hybrids by living radical polymerization of hydroxylated monomers. *Polymer Chemistry* **2011,** *2* (2), 270-288.
90. Hwang, S.-H.; Thielbeer, F.; Jeong, J.; Han, Y.; Chankeshwara, S. V.; Bradley, M.; Cho, W.-S., Dual contribution of surface charge and protein-binding affinity to the cytotoxicity of polystyrene nanoparticles in nonphagocytic A549 cells and phagocytic THP-1 cells. *Journal of Toxicology Environmental Health, Part A* **2016,** *79* (20), 925-937.
91. Kalluru, R.; Fenaroli, F.; Westmoreland, D.; Ulanova, L.; Maleki, A.; Roos, N.; Madsen, M. P.; Koster, G.; Jacobsen, W. E.; Wilson, S., Polylactide-co-glycolide-rifampicin-nanoparticles efficiently clear Mycobacterium bovis BCG infection in macrophages and remain membrane-bound in phago-lysosomes. *Cell Sci* **2013**, jcs. 121814.
92. Patel, B.; Gupta, N.; Ahsan, F., Particle engineering to enhance or lessen particle uptake by alveolar macrophages and to influence the therapeutic outcome. *European Journal of Pharmaceutics Biopharmaceutics* **2015,** *89*, 163-174.
93. Pei, Y.; Yeo, Y., Drug delivery to macrophages: Challenges and opportunities. *Journal of Controlled Release* **2016,** *240*, 202-211.
94. Filatova, L. Y.; Klyachko, N. L.; Kudryashova, E. V., Targeted delivery of anti-tuberculosis drugs to macrophages: targeting mannose receptors. *Russian Chemical Reviews* **2018,** *87* (4), 374.
95. Park, J. S.; Lee, J.-Y.; Lee, Y. J.; Kim, S. J.; Cho, Y.-J.; Yoon, H. I.; Lee, C.-T.; Song, J.; Lee, J. H., Serum levels of antituberculosis drugs and their effect on tuberculosis treatment outcome. *Antimicrobial Agents Chemotherapy* **2016,** *60* (1), 92-98.
96. Seth, V.; Beotra, A.; Seth, S.; Semwal, O.; Kabra, S.; Jain, Y.; Mukhopadhya, S., Serum concentrations of rifampicin and isoniazid in tuberculosis. *Indian Pediatrics* **1993,** *30* (9), 1091-1098.
97. Horváti, K.; Bacsa, B.; Kiss, E. v.; Gyulai, G.; Fodor, K.; Balka, G.; Rusvai, M. s.; Szabó, E. r.; Hudecz, F.; Bősze, S., Nanoparticle encapsulated lipopeptide conjugate of antitubercular drug isoniazid: in vitro intracellular activity and in vivo efficacy in a Guinea pig model of tuberculosis. *Bioconjugate Chemistry* **2014,** *25* (12), 2260-2268.
98. Toma, C. C.; Aloisi, A.; Bordoni, V.; Di Corato, R.; Rauner, M.; Cuniberti, G.; Delogu, L. G.; Rinaldi, R., Immune Profiling of Polysaccharide Submicron Vesicles. *Biomacromolecules* **2018,** *19* (8), 3560-3571.
99. Richards, S. J.; Jones, A.; Tomás, R. M.; Gibson, M. I., Photochemical "In-Air" Combinatorial Discovery of Antimicrobial Co-polymers. *Chemistry–A European Journal* **2018**.
100. Li, W.-J.; Tang, X.-F.; Shuai, X.-X.; Jiang, C.-J.; Liu, X.; Wang, L.-F.; Yao, Y.-F.; Nie, S.-P.; Xie, M.-Y., Mannose receptor mediates the immune response to Ganoderma atrum polysaccharides in macrophages. *Journal of Agricultural Food Chemistry* **2017,** *65* (2), 348-357.
101. Kuroki, A.; Sangwan, P.; Qu, Y.; Peltier, R.; Sanchez-Cano, C.; Moat, J.; Dowson, C. G.; Williams, E. G.; Locock, K. E.; Hartlieb, M., Sequence Control as a Powerful Tool for Improving the Selectivity of Antimicrobial Polymers. *ACS Applied Materials Interfaces* **2017,** *9* (46), 40117-40126.
102. Phillips, D. J.; Harrison, J.; Richards, S.-J.; Mitchell, D. E.; Tichauer, E.; Hubbard, A. T.; Guy, C.; Hands-Portman, I.; Fullam, E.; Gibson, M. I., Evaluation of the antimicrobial activity of cationic polymers against mycobacteria: Toward antitubercular macromolecules. *Biomacromolecules* **2017,** *18* (5), 1592-1599.

103. Richards, S.-J.; Isufi, K.; Wilkins, L. E.; Lipecki, J.; Fullam, E.; Gibson, M. I., Multivalent Antimicrobial Polymer Nanoparticles Target Mycobacteria and Gram-Negative Bacteria by Distinct Mechanisms. *Biomacromolecules* **2017,** *19* (1), 256-264.
104. Passarini, I.; Rossiter, S.; Malkinson, J.; Zloh, M., In silico structural evaluation of short cationic antimicrobial peptides. *Pharmaceutics* **2018,** *10* (3), 72.
105. Varkouhi, A. K.; Scholte, M.; Storm, G.; Haisma, H. J., Endosomal escape pathways for delivery of biologicals. *Journal of Controlled Release* **2011,** *151* (3), 220-228.
106. Roehm, N. W.; Rodgers, G. H.; Hatfield, S. M.; Glasebrook, A. L., An improved colorimetric assay for cell proliferation and viability utilizing the tetrazolium salt XTT. *Journal of Immunological Methods* **1991,** *142* (2), 257-265.